Communications Earth & Environment https://doi.org/10.1038/s43247-026-03858-5

Article in Press

Fire weather waves drive extreme fires globally

Received: 16 December 2025

Accepted: 20 July 2026

Published online: 23 July 2026

Cite this article as: Yin, C., Abatzoglou, J.T., Jain, P. *et al.* Fire weather waves drive extreme fires globally. *Commun Earth Environ* (2026). https://doi.org/10.1038/s43247-026-03858-5

Cong Yin, John T. Abatzoglou, Piyush Jain, Mojtaba Sadegh, Mike D. Flannigan & Matthew W. Jones

Fire weather waves drive extreme fires globally

Cong Yin[1,2]*, John T. Abatzoglou[3], Piyush Jain[4], Mojtaba Sadegh[5], Mike D. Flannigan[6], Matthew W. Jones[7]

1. Sierra Nevada Research Institute, University of California, Merced, CA, USA
2. State Key Laboratory of Resources and Environment Information System, Institute of Geographic Sciences and Natural Resources Research, Chinese Academy of Sciences, Beijing, China
3. Department of Management of Complex Systems, University of California, Merced, CA, USA
4. Northern Forestry Centre, Canadian Forest Service, Natural Resources Canada, Edmonton, Alberta, Canada
5. Department of Civil Engineering, Boise State University, Boise, ID, USA
6. Department of Natural Resource Science, Thompson Rivers University, Kamloops, British Columbia, Canada
7. Tyndall Centre for Climate Change Research, School of Environmental Sciences, University of East Anglia, Norwich, UK

* Corresponding author: Cong Yin (congyin@ucmerced.edu)

Abstract

We define fire weather waves as persistent extreme fire weather, which can intensify fire activity by sustaining exceptionally warm, dry, and windy conditions. Here, we use daily fire weather index, fire activity, and meteorological data to examine the impacts of fire weather waves on fires, as well as their patterns and trends across global terrestrial ecoregions. Fire weather waves account for only 4% of days but coincide with 26% of the area burned and nearly half of the top 1% most energetic fires in forested ecoregions. Compared with grassland and shrubland fires, forest fires exhibit a larger and more persistent increase in daily burned area in response to fire weather waves, particularly in Mediterranean forests. Fire weather wave frequency has significantly increased across most burnable lands during 1979–2024. Climate projections indicate that fire weather waves will increase throughout the 21st century. These findings underscore fire weather waves as an essential component of early warning systems to strengthen preparedness for extreme fires.

1. Introduction

Despite ongoing declines in global burned area driven by agricultural expansion in fire-prone African savannas [1], increases in extreme fires and regional large fire seasons in forested areas have been documented [2,3], resulting in severe societal and ecological consequences [4–6]. Heightened fire activity is associated with extreme fire weather, characterized by dry, warm, and often windy conditions that enhance fuel dryness and promote fire spread, particularly in flammability-limited temperate and boreal forests [7]. Recent studies have shown increased frequency of extreme fire weather and longer fire weather seasons across much of the global burnable lands, primarily driven by rising temperatures and declining relative humidity [8]. Anthropogenic climate change has already amplified, and is projected to further intensify, extreme fire weather [9,10]. Several studies have examined spatially compounding extreme fire weather or synchronous fire weather, given it can strain fire suppression resources and degrade regional air quality [11–13]. Yet, fewer studies have considered the role of temporally compound extremes on fire [14,15].

Here, we introduce the concept of fire weather waves (FWWs), akin to the definition of heatwaves [16], to emphasize the temporally compounding nature of extreme fire weather [17], which has not been investigated at the global scale. FWWs are persistent episodes of extreme fire weather, which differ from shorter-term extremes that lack sustained conditions conducive to heightened fire activity. We define FWWs as periods when the daily fire weather index (FWI) exceeds the ecoregion-specific 95th percentile threshold (FWI95) for at least three consecutive days, with thresholds calculated from the 1979–2024 daily record. By maintaining favorable conditions for ignition and burning over multiple consecutive days, FWWs heighten fire danger and compound fire growth potential. Examples of FWWs include the widespread persistent extreme fire weather that triggered synchronous burning across both western and eastern Canada, producing exceptional burned area during the 2023 fire season [18], and with the catastrophic fires in Southern California in January 2025 (Fig. S1).

More frequent compound heatwave–drought events, such as those associated with soil moisture deficits [19], may facilitate conditions favorable to FWWs. Hot and dry extremes exhibit inherent spatiotemporal synchronicity, driven by large-scale circulation patterns and local land–atmosphere feedbacks [20]. Persistent high-pressure systems inhibit precipitation, producing prolonged periods of hot and dry conditions that accelerate fuel desiccation [21]. Dry land surfaces further amplify heat extremes by suppressing evaporative cooling, forming a self-reinforcing feedback loop [22]. Climate change intensifies these processes by increasing the frequency and severity of heat extremes and accelerating soil moisture depletion, thereby exacerbating drought conditions [23], although the role that climate change has on persistent circulation patterns is less well established [24]. Strong winds are also implicated in some of the deadliest fires in recent years, as fast-moving flames can overwhelm evacuation and suppression efforts, as seen in the 2024 Chile fires and the 2025 Los Angeles fires, which resulted in at least 137 and 31 fatalities, respectively [5,25]. As a compound manifestation of fire-conducive conditions, including high temperatures, dryness, and strong winds over multiple consecutive days, FWWs potentially play a critical role in promoting fire spread.

Using daily FWI derived from the ERA5 reanalysis (European Centre for Medium-Range Weather Forecasts, Reanalysis v5) [26] and daily burned area and Global Fire Atlas data derived from the MODIS (Moderate Resolution Imaging Spectroradiometer, MCD64A1 Version 6.1) [27,28], we examine the relationship between FWWs and fire activity, as well as the patterns and trends of FWWs across global terrestrial ecoregions (Fig. S2A). Specifically, we first quantify the contribution of FWWs to various measures of fire activity (i.e., daily burned area, number of fires, number of extreme fires codified by size, fire radiative power, and maximum daily spread area). Next, we investigate how FWWs influence fire activity by comparing daily burned area and weather conditions during FWWs with those immediately before and after. Finally, we quantify observed and projected changes in FWW patterns across the globe.

2. Results

2.1 FWWs strongly influence fire activity

FWWs are strongly associated with fire activity, particularly in forested areas. In forest ecoregions during 2002–2024, although FWW days accounted for only 4% of all days (mean across forest ecoregions), 18% of individual fires in the Global Fire Atlas ignited during FWW events (Fig. 1A), and 26% of the total burned area recorded in the MCD64A1 product occurred during FWW events (Fig. 1B). FWWs have played an increasingly important role in fire growth, particularly in the tropical forests of South America and Africa, where the proportion of fires ignited during FWW events increased by more than 20% during 2002–2024 (Fig. S3A). Globally, the proportion of burned area occurring during FWW events increased significantly, by about 5% per decade in forest ecoregions (Fig. S3B). The relationship between FWWs and the most extreme fires is even stronger. Across forest ecoregions during the same period, 30%, 46%, and 30% of the top 1% of largest, most energetic, and fastest-spreading fires, respectively, ignited during FWW events (Figs. 1C, 1D, S3C). Similarly, 34% of the top 1% of days with the highest ecoregion burned area coincided with FWW days (Fig. S3D).

Due to their temporally compounding nature, FWWs exert a stronger influence on fire growth than isolated extreme fire weather (IEFW) days, which are defined here as days with FWI exceeding FWI95 but not part of FWW events. Averaged across forest ecoregions, the daily mean burned area on FWW days is 3.43 times that on IEFW days (Fig. 1E). Similarly, in non-forest ecoregions, daily mean burned area on FWW days is 2.43 times that on IEFW days. Burned area in forest and non-forest ecoregions responds differently to FWWs: across boreal, temperate, and tropical forest ecoregions, there is a strong interannual correlation between total burned area and the number of FWW days, whereas most non-forest ecoregions show weak correlations (Fig. 1F).

2.2 FWW and fuel characteristics shape fire response patterns

Fire activity increases notably during FWWs compared to the days immediately preceding the events. The daily mean ecoregion burned area during FWW events is 2.71 times higher than the pre-FWW average (the three days preceding FWW onset) in forest ecoregions and 1.85 times higher in non-forest ecoregions (Fig. 2A). During the three days following the cessation of FWWs, daily mean ecoregion burned area remained higher than the pre-FWW average in most forest ecoregions but returned to near pre-FWW levels in most non-forest ecoregions, indicating that FWWs exert more persistent impacts on burned area in forest ecoregions (Fig. 2B). Compared with IEFW events (Fig. S4), burned area shows stronger increase following FWW onset, peaking two to six days later, with a more intense and prolonged response in forest ecoregions compared with non-forest ecoregions (Fig. 2E–F). The impact of FWWs on burned area varied across biomes (Table S1). Mediterranean forests exhibited the strongest response, with the daily ecoregion burned area two to six days after FWW onset exceeding the pre-FWW average by more than threefold.

We show an amplified response of burned area to both longer and more severe FWWs. The duration and severity of FWW events are strongly correlated with the maximum daily burned area observed during those events across most ecoregions, highlighting the potential of longer and more intense FWWs to drive extreme fires (Fig. 2C–D). Here, duration refers to the length of a FWW event, and severity to the maximum FWI anomaly relative to the climatological mean over the event period.

2.3 FWWs exacerbate fires through prolonged favorable weather conditions

Widespread warmer, drier, and windier conditions are observed during FWWs. In higher latitudes, the average daily maximum temperature during FWW events is 2–5 °C higher than the three-day pre-FWW average (Fig. 3A). Mid-latitudes experience stronger winds during FWWs, with increases in wind speed being greater in non-forest ecoregions than in forest ecoregions (Fig. 3C), leading to an abrupt increase in fire danger (Fig. 3D).

With the onset of FWWs, daily maximum temperature, vapor pressure deficit, wind speed, and FWI rise sharply, peaking 2–4 days after onset and remaining elevated throughout the FWW period (Fig. 3E). These meteorological and fire weather variables also increase during IEFWs but quickly drop below or near pre-event levels, creating cooler and moister conditions that are less favorable for fire spread and facilitate firefighting efforts.

2.4 FWWs are increasing in frequency, persistence, and severity

FWWs occur most frequently in boreal and tropical regions, where the annual average number of FWW days accounts for over 60% of all extreme fire weather days and exceeds 14 days annually during 1979–2024 (Fig. 4A). The average duration of FWWs is generally less than 7 days across most regions but can surpass 13 days in parts of the tropics. FWWs also exhibit greater relative severity in boreal and tropical regions, where the mean maximum FWI anomaly of events (see Methods) exceeds three standard deviations above local climatological means.

FWW frequency increased significantly across most burnable lands globally, including regions that have recently experienced catastrophic fires such as the western United States, Europe, and South America ($p < 0.05$; Fig. 4B). The strongest trend, exceeding six additional FWW days per decade, is observed in southern Europe, the Amazon and central Africa, while South Asia has seen a decline. Over the past four decades, FWWs in South America and parts of the western United States and southern Europe have become not only more frequent but also more severe.

FWWs are projected to increase throughout the 21st century (Fig. 4C–E). Under the middle-of-the-road pathway (SSP2-4.5), which represents a moderate emissions trajectory consistent with current policies, the global average frequency, duration, and severity of FWWs are projected to increase by 56% (interquartile range: 39%–72%), 17% (14%–22%), and 4% (3%–6%), respectively, during 2041–2070 (the mid-century period) compared with 1991–2020 (the present-day baseline). More regions are projected to experience both more frequent and more severe FWWs. In particular, southern and eastern Europe, Siberia, and parts of South America and southern Africa are likely to emerge as global FWW hotspots (Fig. S5B).

3. Discussion

Previous studies have highlighted the role of fire weather in driving extreme fires [3,29]. Here, we demonstrate that the temporally compounding nature of extreme fire weather, namely fire weather waves (FWWs), not only exert a greater influence on total fire activity than isolate days with high FWI but are also more strongly associated with the most extreme fires. Events such as the catastrophic Southern California fires in January 2025, with an FWW event coinciding with the Palisades, Eaton, and Hurst fires in Los Angeles County (Fig. S1), illustrate the value of early warning systems in anticipating such extremes [30].

We find that FWWs are more strongly associated with vegetation fires in forested areas than in non-forested areas. In most forest ecoregions, more than 30% of fires with the top 1% size or fire radiative power ignited during FWW events, and over 40% of the days with the largest 1% daily ecoregion burned area coincided with FWWs, underscoring the critical role of FWWs in both the ignition and spread of extreme fires. Several factors likely explain this pattern. First, high-productivity forests are generally cooler and moister, with higher soil and fuel moisture and more abundant fuel [31–33], making forest fires more sensitive to prolonged extreme fire weather. In contrast, grasslands and shrublands are typically drier, more flammable, and limited by fuel availability, reducing their sensitivity to FWWs. Second, forest fires usually burn for longer periods and exhibit significant inertia [27], which extends the time window during which FWWs can promote fire spread both during and after their occurrence. In contrast, grassland and shrubland fires, which burn rapidly and quickly deplete available fuels [34,35], show both reduced sensitivity to FWWs and have limited influence on burned area immediately post-FWW.

The way fire activity responds to the occurrence, duration, and severity of FWWs varies across the biomes examined in this study. Burned area in Mediterranean forests and shrublands located in the western United States, southern Europe, and southern Australia is most sensitive to FWWs. In these regions, dense human populations increase the frequency of human-caused ignitions, abundant winter and spring precipitation promote vegetation growth and increase fuel loads, and hot-dry summers reduce fuel moisture, creating the necessary conditions for fire spread [36]. FWWs also likely lead to extended daily burn periods, sustaining fires not only across multiple days but also overnight [37]. While these Mediterranean ecosystems have high levels of fire suppression resources that may constrain fire activity and reduce its response to FWWs, the efficacy of this management becomes limited during widespread and prolonged periods of extreme fire weather. This limitation contributes to the disproportionate number of global extreme fire disasters that occur in these regions [38]. Burned area in boreal forest is also very responsive to FWWs, with a greater proportion of fires occurring during FWWs. This pattern reflects the dual constraints of ignition and weather. On one hand, lightning is a major driver of boreal forest fires [39], meaning fires can be constrained by ignition availability under FWWs, thereby reducing their direct response to FWWs. On the other hand, although the fire season, defined as the period during which most of the annual burned area occurs, has been lengthening in parts of the boreal forests, it generally lasts less than three months and is concentrated between June and August [40], which increases the likelihood of fire–FWW concurrence. Tropical coniferous forests in Central America, South Asia, and Southeast Asia have substantial fuel loads, and because FWWs strongly overlap with the dry season when agricultural activities increase ignition loads [41], these forests display pronounced sensitivity to FWWs. Fire activity in the tropical forests of South America and Africa increasingly occurs during FWW events, driven by a significant increase in extreme fire weather conditions [42,43].

FWWs intensify extreme fire danger by sustaining warmer, drier, and windier conditions that lower fuel moisture and facilitate fire spread. Over the past four decades, the frequency, duration, and severity of FWWs have increased markedly at the global scale. In regions such as South America, and parts of the western United States and southern Europe, FWWs have become not only more frequent but also more severe. Projections indicate that FWWs will continue to increase throughout the 21st century. These findings are consistent with prior research on extreme fire weather [8,12], while emphasizing the growing temporally compound nature of fire weather extremes.

There are three main limitations to this study. First, uncertainties may arise from errors and biases in the fire data. The MCD64A1 burned area product tends to underestimate small fires in low-biomass regions [28]. Slow-spreading fires can be over-segmented by the Global Fire Atlas algorithm due to large gaps in burn dates between adjacent cells, and the accuracy of burn-date estimates declines in high-biomass regions [27]. These issues can affect analyses based on daily-scale fire observations. Second, relying on a single ensemble realization for each CMIP6 model used for FWW projections restricts our ability to fully quantify the influence of internal climate variability and likely inflates the range of forced changes across models [44]. Third, our investigation of the relationship between FWWs and fire activity has been conducted at the daily and ecoregion/biome scales, which limits the ability to fully capture continuous diurnal fire dynamics (e.g., limited nighttime humidity recovery that favors extreme fires) and primarily reflects the bioclimatic features of FWW–fire interactions. Future work could incorporate factors such as fuel availability and ignition sources, and focus on specific highly intense fires, such as pyrocumulonimbus events, at finer spatial and temporal (e.g., sub-daily) resolutions, supported by more comprehensively validated fire datasets.

Our findings highlight FWWs as a critical driver of fire activity, particularly in driving extreme fires in forest ecosystems. Mediterranean forests in the western United States, southern Europe, and southern Australia emerge as especially responsive to FWWs, suggesting that monitoring and forecasting FWWs can provide a valuable addition to early warning systems, enhancing the capacity to anticipate extreme fires in the world's most fire-prone landscapes. Incorporating FWW information into preparedness and response strategies is therefore essential, not only to protect human lives and property but also to mitigate the cascading ecological and climatic impacts of large wildfires.

4. Materials and Methods

4.1 Fire, fire weather index, and meteorological data

We used daily burned area data and the Global Fire Atlas for 2002–2024 to investigate the relationship between fire activity and fire weather waves (FWWs). The daily burned area was derived from the MCD64A1 product [28], which provides the date of burn for each 500 m grid cell. We calculated the burned area for each calendar day (in km^2) and aggregated the results to a 0.25° spatial resolution. The Global Fire Atlas provides the time and location of ignitions, perimeters, size, duration, spread, and direction of each individual fire, also derived from the MCD64A1 product [27]. In addition to these precomputed variables, we further calculated the maximum daily spread area and total fire radiative power (FRP) for each individual fire. The maximum daily spread area was derived from a vectorized version of MCD64A1 that provides burned polygons for each calendar day. Each burned polygon was matched to a unique fire based on its time and location, and the largest daily burned area was taken as the fire's maximum spread area. This differs from the "spread" field in the Global Fire Atlas, which represents the average daily spread area over the duration of each fire event.

The total FRP was obtained from MODIS MCD14DL, which records the FRP at the center point of each 1 km pixel [45]. FRP points were matched to their corresponding fires based on spatial and temporal overlap, and their values were summed to obtain each fire's total FRP. When multiple satellite passes occurred within the same day or night, only the pass with the highest FRP per day was retained to avoid duplication [2]. Ultimately, about 30% of fires were matched with FRP information, primarily because (i) GFA fires are aggregated from MCD64A1 burned area data (500 m resolution), whereas MCD14DL is based on MODIS active fire detections (1 km resolution), so small or edge fires may not be detected as active fire pixels; and (ii) some fires were identified as burned areas but their radiative energy did not exceed the detection threshold for active fire detection. FRP match rates in most ecoregions vary from 10% to 40% (Fig. S6), and fires with FRP data tend to be larger events (e.g., 23% of 1-km^2 fires had matching FRP, whereas 80% of 10-km^2 fires had FRP). Consequently, while smaller fires are underrepresented, this subset provides a robust and highly representative foundation for analyzing extreme energetic fires.

Fire weather index (FWI) provides an internationally used relative measure of the potential fire behavior, reflecting current weather conditions for fire risk [46]. Although the buildup index, calculated based on the drought code and duff moisture code, provides the background state of fuel dryness, the FWI is also driven by the initial spread index, which is highly responsive to fast-changing variables like wind speed and fine fuel moisture content [47], and thus reflects short-term fire weather. To detect FWW events, we calculated daily FWI at 0.25° resolution for 1979–2024 using ERA5 reanalysis data from the European Centre for Medium-Range Weather Forecasts (ECMWF) [26]. The calculation was based on daily maximum temperature, daily minimum relative humidity, daily mean wind speed, and daily total precipitation, with an overwintering procedure applied to account for inter-seasonal drought in cold climates, following prior studies [3,48]. Although the FWI system is ideally computed using meteorological conditions at local noon, we used daily aggregated variables to maintain consistency with the temporal resolution of the Coupled Model Intercomparison Project Phase 6 (CMIP6) model outputs. We also calculated daily mean vapor pressure deficit (VPD) from ERA5 daily mean temperature and dewpoint temperature using the standard formulation based on the difference between saturation and actual vapor pressure [49]. VPD, together with daily maximum temperature and daily mean wind speed, was then used to examine how FWWs modify weather and fuel conditions to influence fire activity.

To estimate future changes in FWWs, we calculated daily FWI from 14 CMIP6 Global Climate Models (GCMs)—ACCESS-CM2, CMCC-ESM2, CNRM-CM6-1, CNRM-ESM2-1, CanESM5, EC-Earth3, EC-Earth3-Veg-LR, INM-CM4-8, IPSL-CM6A-LR, MIROC-ES2L, MIROC6, MPI-ESM1-2-HR, MPI-ESM1-2-LR, and MRI-ESM2-0—under the historical period (1979–2014) and two future scenarios (SSP1-2.6 and SSP2-4.5, 2015–2100). We regridded all datasets to a common 1° resolution to account for the coarser native resolution of the CMIP6 models. Because the FWI calculation requires multiple daily inputs, including maximum temperature, minimum relative humidity, mean wind speed, and total precipitation, the availability of ensemble members providing this exact combination is highly unbalanced across CMIP6 models [43]. Consequently, we used a single ensemble member (r1i1p1f1) for each GCM to ensure equal weighting across all independent GCMs, thereby maintaining a balanced sampling of model structural uncertainty when calculating the multi-model mean. FWW metrics were subsequently computed for each model individually, and the multi-model mean and spread were reported to characterize the ensemble projections.

To better differentiate the roles of vegetation and climate in fire–FWW interactions, we conducted the analysis across 846 global terrestrial ecoregions [50], although the use of static boundaries might miss the continuous spatial movement of persistent high-pressure systems that drive FWWs. These are classified into 454 forest ecoregions and 280 non-forest ecoregions based on their respective biomes, and into 113 unburnable ecoregions if burnable wildland areas (forests, mixed cover, woodlands, shrublands, and grasslands) account for less than 10%, as determined by the Global Land Data Assimilation System (GLDAS) vegetation map. This 10% threshold is informed by global land cover classification definitions (e.g., International Geosphere-Biosphere Programme, University of Maryland), where areas with less than 10% vegetation cover are classified as ' barren or sparsely vegetated' [51,52], indicating they lack sufficient fuel continuity to sustain fire spread. All the above-mentioned daily gridded data were summed (for burned area) or averaged (for other variables) to the corresponding ecoregion.

4.2 Definition of ecoregion-level FWWs

FWWs refer to persistent extreme fire weather. Based on the ecoregion-averaged daily FWI, extreme fire weather days are defined as those when FWI exceeds the 95th percentile (FWI95), calculated over the full study period (1979–2024) for each ecoregion. Building on the concepts of heatwaves and thirstwaves [16,53], and given that the mean duration of extreme fire weather ranges from two to four days across most ecoregions (Fig. S7), we defined an FWW as extreme fire weather lasting for at least three consecutive days. For comparison, isolated extreme fire weather (IEFW) was defined as extreme fire weather events with a duration of fewer than three consecutive days, ensuring consistency with the event-based definition used for FWW.

We also present results based on alternative thresholds to test sensitivity (Figs. S8–S11). Specifically, we tested (i) a fixed FWI95 with extended duration thresholds of five and seven days, and (ii) a fixed three-day duration threshold with varying intensity percentiles of FWI90 and FWI98. The results based on different threshold combinations show consistent fire-FWW relationship patterns (e.g., fire activity in forested ecoregions is more strongly linked to FWWs compared to non-forested ecoregions). As expected, a greater overall fraction of burned area and extreme fires is observed during FWWs when using lower thresholds, since these criteria inherently identify more FWW days.

We applied the same method to detect FWWs using 14 CMIP6 GCMs. Specifically, for each model and SSP scenario, we defined 1979–2024 as the reference period for calculating FWI95 to maintain consistency with the ERA5-based calculations, drawing on data from the model's historical simulation (1979–2014) together with data from the corresponding scenario simulation (2015–2024). Incorporating these early scenario years elevates the FWI95 threshold, thereby making our future projections more conservative. FWWs were then identified separately for each model–scenario combination using its specific FWI95 threshold. Although individual CMIP6 models exhibit identifiable regional biases when simulating the historical mean FWI [54,55] (Fig. S12) and FWW frequency (Fig. S13), the multi-model ensemble captures the primary climatological hotspots observed in the ERA5 reanalysis, justifying its application for future projections. Moreover, since we define FWWs using local percentiles, biases in the baseline climatology may be less consequential than if we used absolute FWI thresholds.

4.3 Quantify the influence of FWWs on fire activity

To evaluate the spatiotemporal dependence between FWWs and fire activity, we quantified the percentage of FWW co-occurrence with all fires, as well as with the top 1% of fires ranked by size, total FRP, and maximum daily spread area from the Global Fire Atlas for each ecoregion during 2002–2024. We also calculated FWW co-occurrence with total burned area (BA) and with the top 1% of BA days from MCD64A1 for each ecoregion during 2002–2024.

To quantify the impact of FWW occurrence, we compared daily mean BA between paired groups: (i) during FWWs vs. during IEFWs; (ii) during FWWs vs. the three days preceding FWWs; and

(iii) during the three days after FWWs vs. the three days preceding FWWs. We used the Mann–Whitney U test to assess within-group differences, given the likely non-normal and skewed distributions of daily BA during 2002–2024. To characterize the BA response to FWW events, we calculated, for each ecoregion, the daily mean BA (averaged across all FWW events) from three days before to twelve days after the FWW onset. The mean BA during the three days preceding the onset was then used as a baseline, and daily BA ratios were computed relative to this baseline. Ecoregion-level ratios were then averaged across ecoregions within each biome to obtain biome-level composites. Ecoregions with a baseline value below 0.25 km^2 (equivalent to one MCD64A1 pixel) were excluded to avoid spuriously large ratio values. To further evaluate the influence of FWW duration and severity, we calculated Pearson correlation coefficients between the maximum daily ecoregion BA during FWW events and event duration and severity for each ecoregion during 2002–2024, with BA log-transformed as $\log_{10}(BA + 10)$ to reduce skewness and limit the influence of extreme values. Here, the duration of a FWW event refers to its total length in days, while the severity represents the maximum FWI anomaly during the event relative to the climatological mean of daily values for 1979–2024, expressed in standard deviations.

We also calculated Pearson correlation coefficients between annual total log-transformed BA and the annual number of FWW days for each ecoregion during 2002–2024. To investigate the mechanisms underlying FWW impacts on fire activity, we compared weather conditions (Tmax, VPD, and wind speed) and FWI between FWW days and the three days preceding FWWs. This short pre-FWW window serves as a control, capturing background conditions within the same season and location while avoiding confounding from longer-term variability. For trend analysis, we applied the modified Mann–Kendall test to account for serial autocorrelation and controlled the false discovery rate using the Benjamini–Hochberg procedure for multiple significance testing [56,57]. All analyses were conducted using Python 3.13.11 and R 4.5.1.

References

1. Andela, N. *et al.* A human-driven decline in global burned area. *Science* **356**, 1356–1362 (2017).
2. Cunningham, C. X., Williamson, G. J. & Bowman, D. M. J. S. Increasing frequency and intensity of the most extreme wildfires on Earth. *Nat Ecol Evol* **8**, 1420–1425 (2024).
3. Abatzoglou, J. T. *et al.* Climate change has increased the odds of extreme regional forest fire years globally. *Nat Commun* **16**, 6390 (2025).
4. Jones, M. W. *et al.* State of Wildfires 2023–2024. *Earth System Science Data* **16**, 3601–3685 (2024).

5. Kolden, C. A., Abatzoglou, J. T., Jones, M. W. & Jain, P. Wildfires in 2024. *Nat Rev Earth Environ* **6**, 237–239 (2025).

6. Teymoor Seydi, S. *et al.* Increasing global human exposure to wildland fires despite declining burned area. *Science* **389**, 826–829 (2025).

7. Jones, M. W. *et al.* Global and Regional Trends and Drivers of Fire Under Climate Change. *Reviews of Geophysics* **60**, e2020RG000726 (2022).

8. Jain, P., Castellanos-Acuna, D., Coogan, S. C. P., Abatzoglou, J. T. & Flannigan, M. D. Observed increases in extreme fire weather driven by atmospheric humidity and temperature. *Nat. Clim. Chang.* **12**, 63–70 (2022).

9. Abatzoglou, J. T., Williams, A. P. & Barbero, R. Global Emergence of Anthropogenic Climate Change in Fire Weather Indices. *Geophysical Research Letters* **46**, 326–336 (2019).

10. Touma, D., Stevenson, S., Lehner, F. & Coats, S. Human-driven greenhouse gas and aerosol emissions cause distinct regional impacts on extreme fire weather. *Nat Commun* **12**, 212 (2021).

11. Abatzoglou, J. T., Juang, C. S., Williams, A. P., Kolden, C. A. & Westerling, A. L. Increasing Synchronous Fire Danger in Forests of the Western United States. *Geophysical Research Letters* **48**, e2020GL091377 (2021).

12. Yin, C. *et al.* Increasing synchronicity of global extreme fire weather. *Science Advances* **12**, eadx8813 (2026).

13. Richardson, D. *et al.* Increasing Fire Weather Season Overlap Between North America and Australia Challenges Firefighting Cooperation. *Earth's Future* **13**, e2024EF005030 (2025).

14. AghaKouchak, A. *et al.* Climate Extremes and Compound Hazards in a Warming World. *Annual Review of Earth and Planetary Sciences* **48**, 519–548 (2020).

15. Kalashnikov, D. A. *et al.* Heatwaves enable wildfire activity in the western United States. *Science Advances* **12**, eaea1277 (2026).

16. Perkins, S. E. & Alexander, L. V. On the Measurement of Heat Waves. *Journal of Climate* **26**, 4500–4517 (2013).

17. Zscheischler, J. *et al.* A typology of compound weather and climate events. *Nat Rev Earth Environ* **1**, 333–347 (2020).

18. Jain, P. *et al.* Drivers and Impacts of the Record-Breaking 2023 Wildfire Season in Canada. *Nat Commun* **15**, 6764 (2024).

19. Tripathy, K. P., Mukherjee, S., Mishra, A. K., Mann, M. E. & Williams, A. P. Climate change will accelerate the high-end risk of compound drought and heatwave events. *Proceedings of the National Academy of Sciences* **120**, e2219825120 (2023).

20. Hosseinzadehtalaei, P., Termonia, P. & Tabari, H. Projected changes in compound hot-dry events depend on the dry indicator considered. *Commun Earth Environ* **5**, 220 (2024).

21. Sharma, A. R., Jain, P., Abatzoglou, J. T. & Flannigan, M. Persistent Positive Anomalies in Geopotential Heights Promote Wildfires in Western North America. *Journal of Climate* **35**, 6469–6486 (2022).

22. Miralles, D. G., Teuling, A. J., van Heerwaarden, C. C. & Vilà-Guerau de Arellano, J. Mega-heatwave temperatures due to combined soil desiccation and atmospheric heat accumulation. *Nature Geosci* **7**, 345–349 (2014).

23. Alizadeh, M. R. *et al.* A century of observations reveals increasing likelihood of continental-scale compound dry-hot extremes. *Science Advances* **6**, eaaz4571 (2020).

24. Pfleiderer, P., Schleussner, C.-F., Kornhuber, K. & Coumou, D. Summer weather becomes more persistent in a 2 °C world. *Nat. Clim. Chang.* **9**, 666–671 (2019).

25. Sadegh, M., Abatzoglou, J. T., AghaKouchak, A. & Seydi, S. T. Ignition matters. *Nat Sustain* **8**, 327–328 (2025).

26. Hersbach, H. *et al.* The ERA5 global reanalysis. *Quarterly Journal of the Royal Meteorological Society* **146**, 1999–2049 (2020).

27. Andela, N. *et al.* The Global Fire Atlas of individual fire size, duration, speed and direction. *Earth System Science Data* **11**, 529–552 (2019).
28. Giglio, L., Boschetti, L., Roy, D. P., Humber, M. L. & Justice, C. O. The Collection 6 MODIS burned area mapping algorithm and product. *Remote Sensing of Environment* **217**, 72–85 (2018).
29. Balch, J. K. *et al.* The fastest-growing and most destructive fires in the US (2001 to 2020). *Science* **386**, 425–431 (2024).
30. AghaKouchak, A. *et al.* Building urban fire resilience to enhance national security. *Nat Cities* **2**, 778–780 (2025).
31. James, S. E., Pärtel, M., Wilson, S. D. & Peltzer, D. A. Temporal heterogeneity of soil moisture in grassland and forest. *Journal of Ecology* **91**, 234–239 (2003).
32. Newberry, B. M. *et al.* Flammability thresholds or flammability gradients? Determinants of fire across savanna–forest transitions. *New Phytologist* **228**, 910–921 (2020).
33. Barberá, I., Paritsis, J., Ammassari, L., Morales, J. M. & Kitzberger, T. Microclimate and species composition shape the contribution of fuel moisture to positive fire-vegetation feedbacks. *Agricultural and Forest Meteorology* **330**, 109289 (2023).
34. Pausas, J. G. & Ribeiro, E. The global fire–productivity relationship. *Global Ecology and Biogeography* **22**, 728–736 (2013).
35. Bedia, J. *et al.* Global patterns in the sensitivity of burned area to fire-weather: Implications for climate change. *Agricultural and Forest Meteorology* **214–215**, 369–379 (2015).
36. Marriner, N. Fire in Mediterranean Ecosystems: ecology, evolution and management. *Méditerranée. Revue géographique des pays méditerranéens / Journal of Mediterranean geography* 111 (2013) doi:10.4000/mediterranee.6936.
37. Luo, K., Wang, X., Castellanos-Acuna, D. & Flannigan, M. A weakened diurnal weather constraint leads to longer burning hours in North America. *Science Advances* **12**, eaed0725 (2026).

38. Cunningham, C. X. *et al.* Climate-linked escalation of societally disastrous wildfires. *Science* **390**, 53–58 (2025).

39. Veraverbeke, S. *et al.* Lightning as a major driver of recent large fire years in North American boreal forests. *Nature Clim Change* **7**, 529–534 (2017).

40. Abatzoglou, J. T., Williams, A. P., Boschetti, L., Zubkova, M. & Kolden, C. A. Global patterns of interannual climate–fire relationships. *Global Change Biology* **24**, 5164–5175 (2018).

41. Le Page, Y., Oom, D., Silva, J. M. N., Jönsson, P. & Pereira, J. M. C. Seasonality of vegetation fires as modified by human action: observing the deviation from eco-climatic fire regimes. *Global Ecology and Biogeography* **19**, 575–588 (2010).

42. Feron, S. *et al.* South America is becoming warmer, drier, and more flammable. *Commun Earth Environ* **5**, 501 (2024).

43. Turco, M. *et al.* The emerging human fingerprint on global extreme fire weather. *Science Advances* **12**, eadx9845 (2026).

44. Lehner, F. *et al.* Partitioning climate projection uncertainty with multiple large ensembles and CMIP5/6. *Earth System Dynamics* **11**, 491–508 (2020).

45. Earth Science Data Systems, N. MODIS/Aqua Terra Thermal Anomalies/Fire locations 1km FIRMS NRT (Vector data) | NASA Earthdata. Earth Science Data Systems, NASA (2025).

46. Wagner, V. & E, C. *Development and Structure of the Canadian Forest Fire Weather Index System*. https://ostrnrcan-dostrncan.canada.ca/handle/1845/228434 (1987).

47. Dowdy, A. J., Mills, G. A., Finkele, K. & de Groot, W. Index sensitivity analysis applied to the Canadian Forest Fire Weather Index and the McArthur Forest Fire Danger Index. *Meteorological Applications* **17**, 298–312 (2010).

48. McElhinny, M., Beckers, J. F., Hanes, C., Flannigan, M. & Jain, P. A high-resolution reanalysis of global fire weather from 1979 to 2018 – overwintering the Drought Code. *Earth System Science Data* **12**, 1823–1833 (2020).

49. Allen, R. G., Pereira, L. S., Raes, D., Smith, M., & others. Crop evapotranspiration-Guidelines for computing crop water requirements-FAO Irrigation and drainage paper 56. *Fao, rome* **300**, D05109 (1998).

50. Dinerstein, E. *et al.* An Ecoregion-Based Approach to Protecting Half the Terrestrial Realm. *BioScience* **67**, 534–545 (2017).

51. Hansen, M. C., Defries, R. S., Townshend, J. R. G. & Sohlberg, R. Global land cover classification at 1 km spatial resolution using a classification tree approach. *International Journal of Remote Sensing* **21**, 1331–1364 (2000).

52. Loveland, T. R. *et al.* Development of a global land cover characteristics database and IGBP DISCover from 1 km AVHRR data. *International Journal of Remote Sensing* **21**, 1303–1330 (2000).

53. Kukal, M. S. & Hobbins, M. Thirstwaves: Prolonged Periods of Agricultural Exposure to Extreme Atmospheric Evaporative Demand for Water. *Earth's Future* **13**, e2024EF004870 (2025).

54. Gallo, C. *et al.* Evaluation of CMIP6 model performances in simulating fire weather spatiotemporal variability on global and regional scales. *Geoscientific Model Development* **16**, 3103–3122 (2023).

55. Zhou, W., Leung, L. R., Harrop, B. E., Chen, Z. & Chang, C.-C. A theoretical index for understanding distinct land relative humidity trends in observations, reanalyses, and models. *Proceedings of the National Academy of Sciences* **123**, e2512645123 (2026).

56. Hamed, K. H. & Ramachandra Rao, A. A modified Mann-Kendall trend test for autocorrelated data. *Journal of Hydrology* **204**, 182–196 (1998).

57. Benjamini, Y. & Hochberg, Y. Controlling the False Discovery Rate: A Practical and Powerful Approach to Multiple Testing. *Journal of the Royal Statistical Society. Series B (Methodological)* **57**, 289–300 (1995).

Data availability

All data used in this study are freely accessible. The MCD64A1 burned area product was obtained from https://doi.org/10.5067/MODIS/MCD64A1.061, and the Global Fire Atlas from https://doi.org/10.5281/zenodo.14065246. The MCD64 monthly shapefiles were accessed via the fuoco SFTP server (Server: fuoco.geog.umd.edu; Login name: fire; Password: burnt), and the MCD14DL active fire shapefiles were downloaded from https://firms.modaps.eosdis.nasa.gov/download/. ERA5 reanalysis data were obtained from https://doi.org/10.24381/cds.4991cf48, and CMIP6 model outputs from https://aims2.llnl.gov/search/cmip6/. The ecoregion shapefile was downloaded from https://ecoregions.appspot.com, and the 0.25° vegetation type dataset from https://ldas.gsfc.nasa.gov/gldas/vegetation-class-mask or https://github.com/SciExtremes/fire-weather-wave/blob/main/GLDASp5_domveg_CLSMF2.5_025d.nc4. A table detailing the forest/non-forest categorization and burnable area fractions for ecoregions is available at https://github.com/SciExtremes/fire-weather-wave.

Acknowledgements

Not applicable.

Funding

J.T.A. and C.Y. were supported by the United States National Science Foundation (OAI-2019762) and the United States Department of the Interior Joint Fire Science Program (L21AC10247).

Author contributions

C.Y. and J.T.A. conceived the study and designed the experiments. C.Y., J.T.A., and P.J. conducted the analyses. C.Y. performed the statistical modeling and data visualization. C.Y. and J.T.A. wrote the initial draft of the manuscript. All authors discussed the results, contributed to the final manuscript, and approved the submitted version.

Competing interests

The authors declare no competing interests.

Figure captions

Fig. 1. FWWs are strongly associated with fire activity during 2002–2024. (A) Percentage of fires ignited during FWW events. (B) Percentage of daily ecoregion burned area (BA) occurring during FWW events. (C) Percentage of fires with top 1% size ignited during FWW events. (D) Same as (C), but for top 1% fire radiative power (FRP). Note that the no-data areas (denoted in white) vary across metrics because some ecoregions lack fires in the top 1% for size or FRP. (E) Ratio of daily mean ecoregion BA on FWW days to that on IEFW days, with dotted regions indicating statistically significant differences ($p < 0.05$, two-sided Mann-Whitney U test, see

Supplementary Data 1 for significance values for each ecoregion). (F) Interannual correlation between FWW days and ecoregion BA, with dotted regions indicating statistically significant correlations ($p < 0.05$, two-sided Pearson correlation test, Supplementary Data 1). Unburnable ecoregions, defined as ecoregions where burnable wildland vegetation accounts for <10% of the area are masked out. The numbers in panels (A)–(D) represent values summed over forest (F) and non-forest (NF) ecoregions, whereas the numbers in the other panels represent mean values ($\bar{\ }$) across F and NF ecoregions. This convention is applied throughout the paper.

Fig. 2. Fire response patterns are influenced by FWWs and fuel characteristics during 2002–2024. (A–B) Ratios of daily mean ecoregion burned area (BA): (A) during FWWs vs. the three days before FWW onset, (B) during the three days after FWW end vs. the three days before FWW onset. Dotted regions indicate statistically significant differences ($p < 0.05$, two-sided Mann-Whitney U test, Supplementary Data 1). (C–D) Pearson correlations between the maximum daily ecoregion BA during FWW events and event (C) duration and (D) severity. Dotted regions indicate statistically significant correlations ($p < 0.05$, two-sided Pearson correlation test, Supplementary Data 1). (E) BA ratio from three days before to twelve days after FWW onset, relative to the three-day pre-onset mean. Thinner lines represent average BA response across ecoregions within each forest biome, while the bold line represents the average across all forest ecoregions. Darker line segments near the beginning indicate the mean FWW duration for the corresponding biomes. (F) Same as (E), but for non-forest biomes. Biome distributions are shown in Fig. S2B.

Fig. 3. FWWs promote burning by sustaining fire-conducive weather conditions. (A) Difference between average daily maximum temperature (Tmax) during FWW events and the three-day pre-FWW average during 1979–2024. (B–D) Same as (A), but for vapor pressure deficit (VPD), wind speed, and FWI, respectively. (E) Difference in these variables from three days before to twelve days after the onset of FWW (solid lines) or IEFW (dashed lines) events, relative to the three-day pre-event average, for forest (dark lines) and non-forest (light lines) ecoregions. Darker segments at the beginning of each line indicate the average duration of FWWs in forest and non-forest ecoregions.

Fig. 4. FWWs are becoming, and are projected to become, more frequent, persistent, and severe. (A) Annual average share of FWW days among all extreme fire weather days, along with FWW frequency (total number of FWW days), duration (mean event length), and severity (mean event-level maximum FWI anomaly) during 1979–2024. (B) Decadal trends of the metrics shown in (A), with dotted regions indicating statistically significant trends ($p < 0.05$, two-sided modified Mann-Kendall test, Supplementary Data 1). The composite map highlights regions with significant positive trends in FWW frequency, duration, and severity. (C–E) Time series of FWW frequency, duration, and severity, averaged across ecoregions using area weighting, based on ERA5 (black) and 14 climate models under the historical (green), SSP1-2.6 (blue), and SSP2-4.5 (red) scenarios. Model-based lines show 5-year smoothed averages to filter out interannual climate variability (e.g., El Niño-Southern Oscillation) while preserving the underlying decadal trends, and shaded areas indicate the inter-model minimum–maximum range.

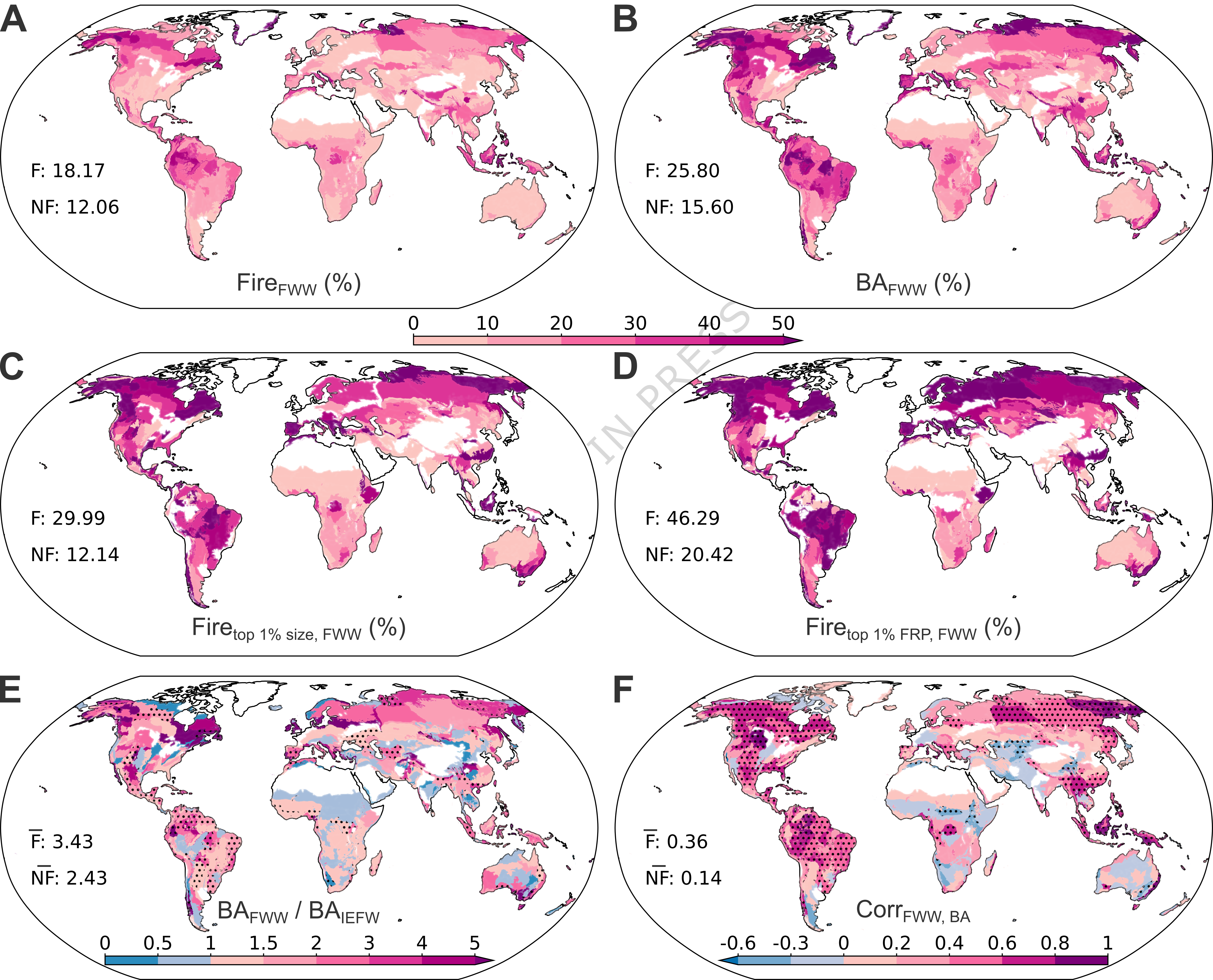

A
F: 18.17
NF: 12.06
Fire$_{FWW}$ (%)
B
F: 25.80
NF: 15.60
BA$_{FWW}$ (%)
0 10 20 30 40 50
C
F: 29.99
NF: 12.14
Fire$_{top\ 1\%\ size,\ FWW}$ (%)
D
F: 46.29
NF: 20.42
Fire$_{top\ 1\%\ FRP,\ FWW}$ (%)
E
$\overline{F}$: 3.43
$\overline{NF}$: 2.43
BA$_{FWW}$ / BA$_{IEFW}$
0 0.5 1 1.5 2 3 4 5
F
$\overline{F}$: 0.36
$\overline{NF}$: 0.14
Corr$_{FWW,\ BA}$
-0.6 -0.3 0 0.2 0.4 0.6 0.8 1

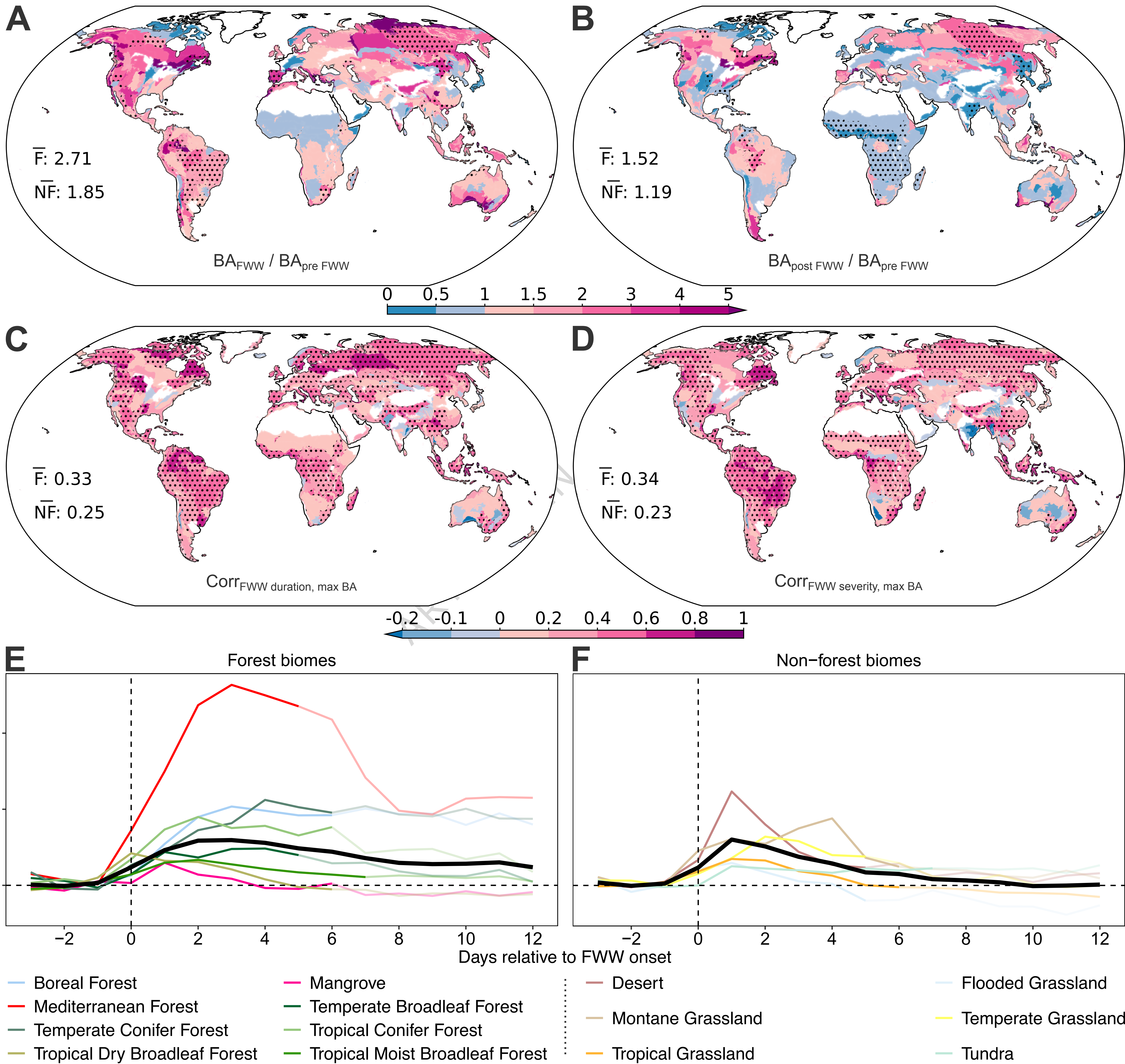
A
F̄: 2.71
NF̄: 1.85
BA_FWW / BA_pre FWW
B
F̄: 1.52
NF̄: 1.19
BA_post FWW / BA_pre FWW
0 0.5 1 1.5 2 3 4 5
C
F̄: 0.33
NF̄: 0.25
Corr_FWW duration, max BA
D
F̄: 0.34
NF̄: 0.23
Corr_FWW severity, max BA
-0.2 -0.1 0 0.2 0.4 0.6 0.8 1
E
Forest biomes
F
Non−forest biomes
BA ratio
Days relative to FWW onset
Boreal Forest
Mediterranean Forest
Temperate Conifer Forest
Tropical Dry Broadleaf Forest
Mangrove
Temperate Broadleaf Forest
Tropical Conifer Forest
Tropical Moist Broadleaf Forest
Desert
Montane Grassland
Tropical Grassland
Flooded Grassland
Temperate Grassland
Tundra

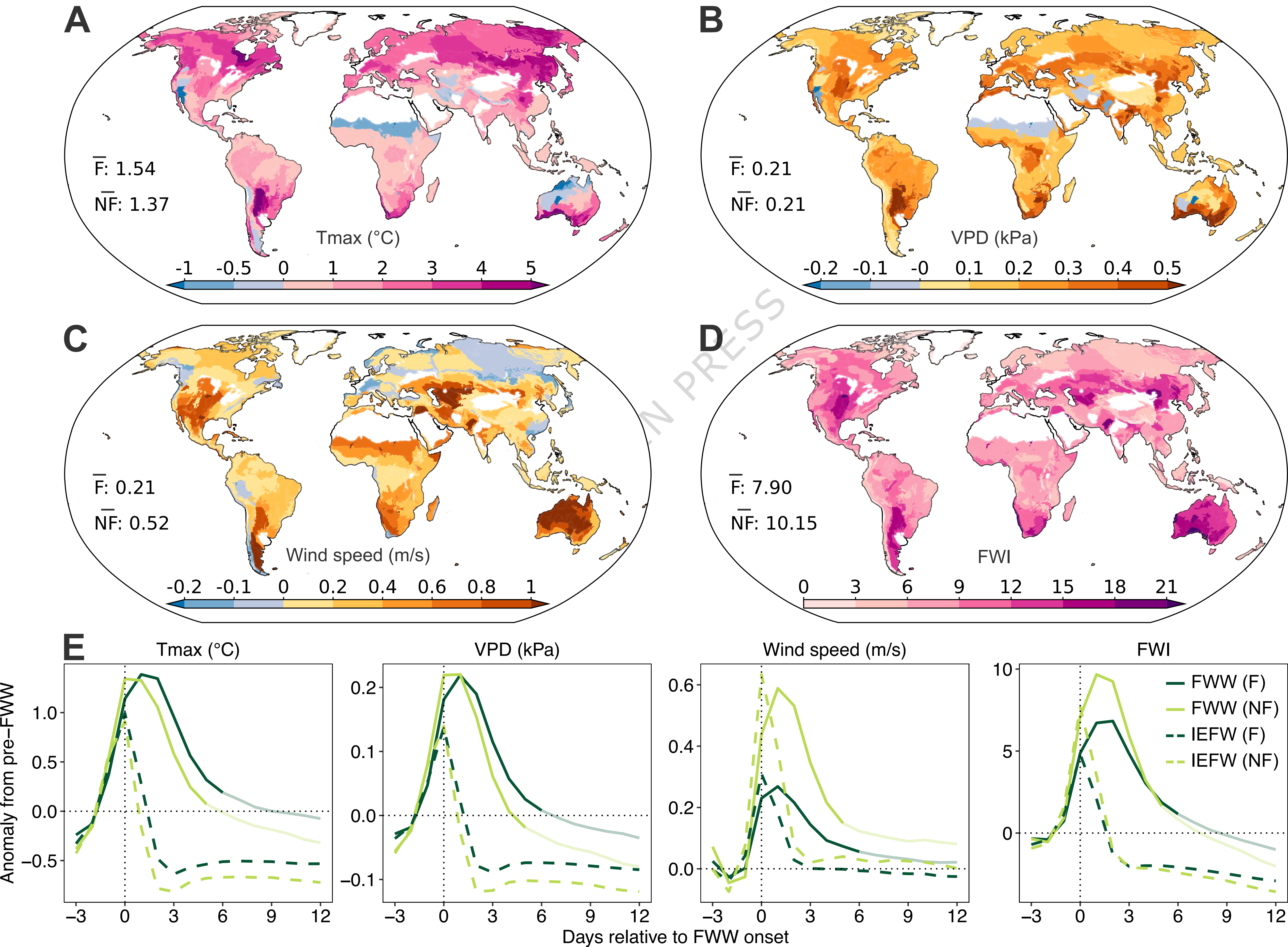
A
$\overline{F}$: 1.54
$\overline{NF}$: 1.37
Tmax (°C)
-1 -0.5 0 1 2 3 4 5
B
$\overline{F}$: 0.21
$\overline{NF}$: 0.21
VPD (kPa)
-0.2 -0.1 -0 0.1 0.2 0.3 0.4 0.5
C
$\overline{F}$: 0.21
$\overline{NF}$: 0.52
Wind speed (m/s)
-0.2 -0.1 0 0.2 0.4 0.6 0.8 1
D
$\overline{F}$: 7.90
$\overline{NF}$: 10.15
FWI
0 3 6 9 12 15 18 21
E
Tmax (°C)
VPD (kPa)
Wind speed (m/s)
FWI
Anomaly from pre–FWW
FWW (F)
FWW (NF)
IEFW (F)
IEFW (NF)
Days relative to FWW onset

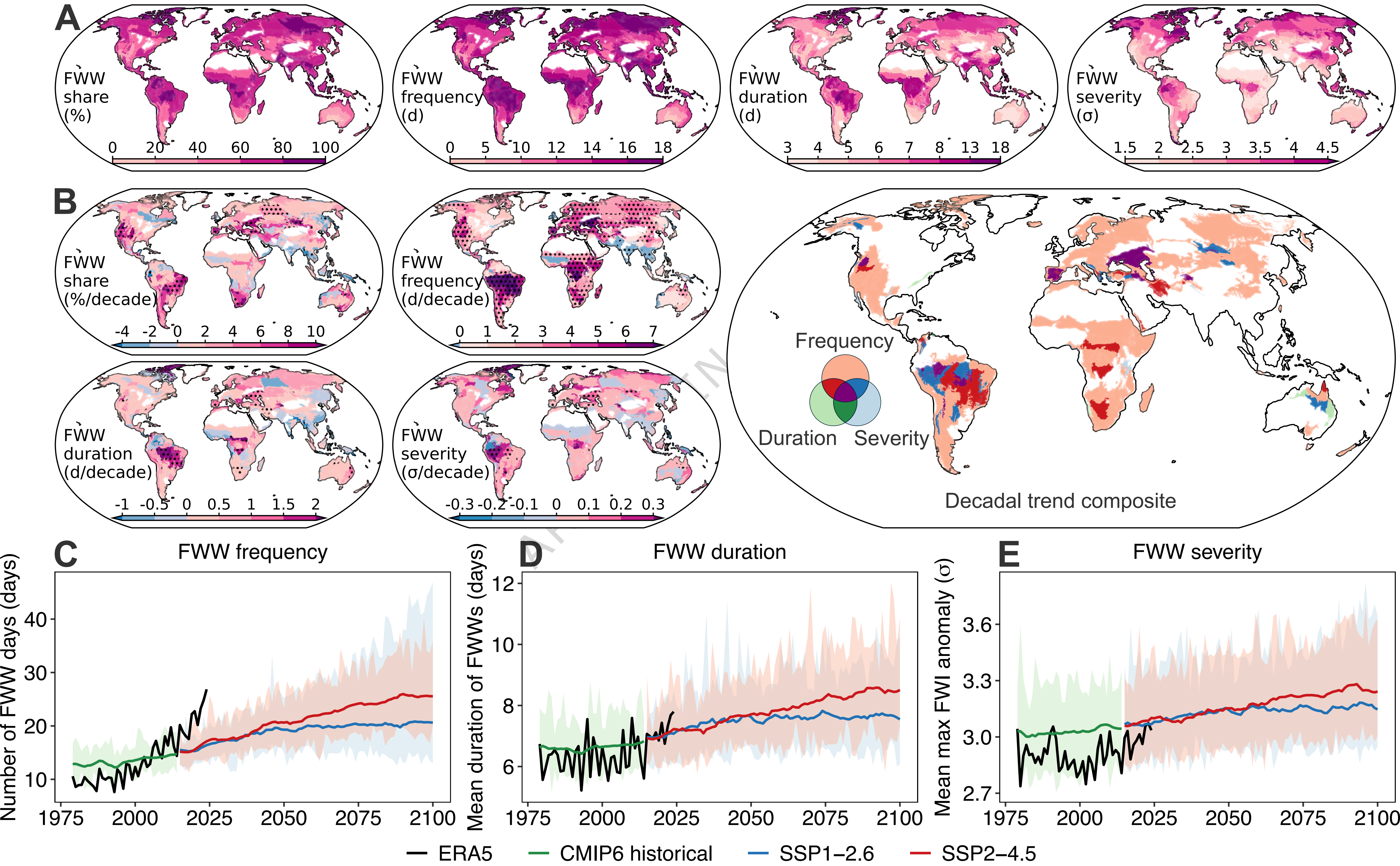
A
FWW share (%)
0 20 40 60 80 100
FWW frequency (d)
0 5 10 12 14 16 18
FWW duration (d)
3 4 5 6 7 8 13 18
FWW severity (σ)
1.5 2 2.5 3 3.5 4 4.5
B
FWW share (%/decade)
-4 -2 0 2 4 6 8 10
FWW frequency (d/decade)
0 1 2 3 4 5 6 7
FWW duration (d/decade)
-1 -0.5 0 0.5 1 1.5 2
FWW severity (σ/decade)
-0.3 -0.2 -0.1 0 0.1 0.2 0.3
Frequency
Duration
Severity
Decadal trend composite
C
FWW frequency
Number of FWW days (days)
D
FWW duration
Mean duration of FWWs (days)
E
FWW severity
Mean max FWI anomaly (σ)
1975 2000 2025 2050 2075 2100
ERA5
CMIP6 historical
SSP1–2.6
SSP2–4.5